PHYSICAL REVIEW A

GENERAL PHYSICS

THIRD SERIES, VOLUME 29, NUMBER 2 FEBRUARY 1984

Search for P and T violations in the hyperfine structure of thallium fluoride

Dean A. Wilkening and Norman F. Ramsey
Lyman Laboratory, Harvard University, Cambridge, Massachusetts 02138

Daniel J. Larson
Beams Laboratory of Physics, University of Virginia, Charlottesville, Virginia 22901
(Received 10 June 1983)

A molecular-beam experiment using TlF is described. The experiment searched for a P- and T-violating interaction of the form $\mathcal{H}_{PT}=d\,\vec{\sigma}_{\mathrm{Tl}}\cdot\vec{\lambda}_{\mathrm{TlF}}$, where d is a coupling constant, $\vec{\sigma}_T$ is a unit vector parallel to the thallium nuclear spin, and $\vec{\lambda}_{\mathrm{TlF}}$ is a unit vector parallel to the TlF internuclear axis. The experiment yields the null result $d/h=8\pm12$ mHz. Interpreting the interaction in terms of an electric dipole moment on the proton, D_p, or in terms of a possible weak neutral-current tensor interaction with a coupling constant C_T, this result corresponds to $D_p=(1.3\pm2.0)\times10^{-21}$ e cm and $C_T=(6\pm9)\times10^{-6}G_F$, where the errors incorporate unexplained systematic effects as well as statistical errors.

I. INTRODUCTION

This paper describes an experiment which searched for a parity (P) and time-reversal (T) violating frequency shift for a hyperfine transition in the TlF molecule when the relative direction of laboratory electric and magnetic fields was reversed. The main interest in this search stems from the test for T violation. Ever since the CP-violating decay of the long-lived kaon ($K_L^0\rightarrow2\pi$) was observed by Christenson, Cronin, Fitch, and Turlay,[1] T violations in other physical systems have eluded observation. (CP violation implies T violation if one invokes the CPT theorem.)

One approach has been to search for an electric dipole moment (EDM) in nondegenerate quantum-mechanical systems, or more specifically, the EDM of elementary particles. The Hamiltonian for the interaction of a particle with spin $\vec{I}$ and electric dipole moment $\vec{D}$, with an electric field $\vec{E}$ is

$$\mathcal{H}_{\mathrm{EDM}}=-\vec{D}\cdot\vec{E}=-\frac{D}{I}\vec{I}\cdot\vec{E}\ .$$

Since this interaction represents an energy, sensitive tests for its presence can be made by searching for small changes in the transition frequency between states with different projections of $\vec{I}$ when an electric field is reversed relative to the axis of spin quantization. For example, in the recent neutron EDM experiments, where the essential physics is easily grasped, the neutron spin is quantized along a laboratory magnetic field giving rise to a neutron magnetic resonance frequency equal to $2\mu_N B/h$, where μ_N is the neutron magnetic moment, B is the magnitude of the external magnetic field, and h is Planck's constant. If one adds a laboratory electric field parallel to the magnetic field, the precessional frequency changes due to the electric dipole interaction. When the electric field is reversed relative to the magnetic field, the transition frequency changes by an amount

$$\Delta\nu=\frac{4D_nE}{h}\ ,$$

where D_n represents the magnitude of the neutron EDM and E, the magnitude of the laboratory electric field. This is the sought-after P- and T-violating frequency shift in the neutron EDM experiments. Since Purcell and Ramsey[2] originally proposed such experiments in 1950, a long line of neutron-beam[3] and neutron-bottle[4] experiments have been conducted. The most sensitive published result so far is the null value $D_n=(2.3\pm2.3)\times10^{-25}$ e cm^4.

An EDM for charged particles is more difficult to measure since the application of the electric field in an experiment similar to the neutron experiments would accelerate the particle out of the apparatus.[2] Using a system which is overall neutral (i.e., an atom or a molecule) at first appears unproductive since, even with the application of an external field, the electric field averages to zero for each charged particle. Schiff[5] formally demonstrated that for a nonrelativistic quantum-mechanical system of point charges, interacting solely by electrostatic forces, no observable effect occurs which is linear in the EDM of the

individual particles. However, as both he and later Sandars[6] have pointed out, relativistic spin-dependent interactions (e.g., magnetic interactions) and finite particle size can give rise to an interaction linear in the EDM. The former figures most prominently in electron EDM experiments, while the latter is most significant for observing the effects of a nuclear EDM in high-Z atoms. Classically one can think of these exceptions in terms of a force which balances the electrostatic force experienced by the charged particle as it samples the nonzero average electric field required to produce a first-order EDM interaction. In the magnetic case the gradient of the magnetic field interacts with the magnetic dipole moment and for finite nuclear sizes the nuclear force balances the electrostatic force on the charged particle whose EDM we wish to observe.

Sandars[7] pursued these exceptions the furthest, turning them into several clever experiments involving the EDM of the electron[8] and proton.[9,10] The latter experiments involving the proton EDM provided the impetus for the experiment reported in this paper.

In this experiment a molecular beam is used to observe the nuclear resonance for ^{205}Tl ($I=\frac{1}{2}$) in TlF in the presence of parallel, then antiparallel, electric and magnetic fields. Any shift in the resonance frequency when the relative direction of the two fields is reversed represents a violation of P and T symmetries. The interaction for such an effect has been written in the form

$$\mathscr{H}_{PT}=d\,\vec{\sigma}_{\mathrm{Tl}}\cdot\vec{\lambda}_{\mathrm{TlF}}\,, \tag{1}$$

where d is a phenomenological constant, $\vec{\sigma}_{\mathrm{Tl}}$ is a unit vector parallel to the Tl nuclear spin, and $\vec{\lambda}_{\mathrm{TlF}}$ is a unit vector parallel to the TlF internuclear axis pointing toward the fluorine nucleus.[10] In the absence of an external electric field this interaction yields zero for any given rotational state since $\vec{\sigma}_{\mathrm{Tl}}$ (which in this case is coupled to the molecular rotation $\vec{\mathrm{J}}$) is perpendicular to $\vec{\lambda}_{\mathrm{TlF}}$. However, with the application of an external electric field the molecule becomes polarized yielding a nonzero expectation value.

The physical significance of Eq. (1) is as follows. Thallium is a spin-$\frac{1}{2}$ nucleus where the spin arises from an unpaired proton in an $S_{1/2}$ orbit, according to the shell model. If a proton EDM exists, the Tl nucleus acquires an EDM. Furthermore the Tl nuclear EDM distribution will essentially be that of the outer unpaired proton spin, whereas the nuclear charge distribution is more nearly uniform. This difference between the nuclear charge and EDM distributions implies that a nonzero electric field can exist on the Tl EDM distribution without violating the constraint that the electric field average to zero over the charge distribution of the nucleus (this is the finite size effect). The magnitude of this effect depends on the difference between the mean-square radii of the charge and EDM distributions, and on the magnitude of the gradients of the electric field at the Tl nuclear site. Combining the finite size and magnetic effects for TlF yields an effective electric field on the order of 24 kV/cm on the unpaired proton pointing along the internuclear axis,[7,10] hence Eq. (1). Owing to molecular rotation, this internal electric field averages to zero. However, in the presence of a 20 kV/cm laboratory electric field, the $J=1$ rotational state of TlF becomes 46% polarized, giving rise to an effective electric field on the proton EDM of 11 kV/cm projected onto a laboratory axis defined by the external electric field. The magnitude of this effective electric field is remarkably large.

Thinking in terms of an effective electric field applied to the unpaired proton EDM within the Tl nucleus provides a simple physical picture. However, a proton EDM is by no means the only origin for the interaction given in Eq. (1). A Tl nuclear EDM could arise from a P- and T-violating nuclear force, quite apart from a proton EDM, though no model for such an effect has been presented. Furthermore, Hinds *et al.*[10,11] have shown that an interaction of this form can arise from a weak neutral-current tensor coupling between electrons and protons. Consequently, the result of this experiment can be used to set upper limits for several interactions.

By analogy with the neutron experiments we might expect that an external magnetic field must be applied to the Tl nucleus to remove the degeneracy of the $m_{\mathrm{Tl}}=\pm\frac{1}{2}$ states. This turns out not to be the case. In TlF an internal magnetic field is generated at the Tl nuclear site due to the rotational motion of the molecule, along with a small contribution from the fluorine magnetic dipole moment. This is the origin of the spin-rotation hyperfine interaction ($c\vec{\mathrm{I}}\cdot\vec{\mathrm{J}}$) and the magnetic dipole-dipole hyperfine interaction, respectively. Therefore, if one state selects the TlF molecules to be in the state $|J=1,m_J=-1,m_1=-\frac{1}{2},m_2=-\frac{1}{2}\rangle$ (using the uncoupled representation, where m_1 denotes the Tl nuclear spin and m_2 the F nuclear spin), a magnetic field on the order of 50 G exists at the Tl nuclear site. Furthermore, the average value of this magnetic field is parallel to the axis of quantization used to determine m_J, m_1, and m_2. By state selecting these "magnetic" quantum numbers for a TlF molecular beam prior to sending the beam through a resonance region in which only an electric field is present, a Tl nuclear resonance,

$$(|m_J=-1,m_1=-\tfrac{1}{2},m_2=-\tfrac{1}{2}\rangle \rightarrow |m_J=-1,m_1=+\tfrac{1}{2},m_2=-\tfrac{1}{2}\rangle)$$

occurs with parallel (or antiparallel) electric and magnetic fields at the Tl nuclear site. That the fields are exactly parallel is guaranteed quantum mechanically because the laboratory electric field provides the quantization axis for the angular momenta. Consequently, both the internal electric and magnetic fields at the Tl nuclear site average to fields whose only nonzero components lie along the direction of the laboratory electric field.

State selecting the opposite magnetic quantum numbers (m_J+1 and $m_2=+\frac{1}{2}$) reverses the internal magnetic field. Experimentally this is accomplished by reversing the direction of a laboratory magnetic field in the state-selecting region. To minimize depolarization of the beam the state-selecting magnetic field is parallel (or antiparallel) to the electric field in the resonance region and precautions were taken to ensure that the molecules pass

adiabatically between the two regions.

Thus, a P and T violation produces a frequency shift in the Tl nuclear resonance when the relative direction of an electric and magnetic field at the Tl nuclear site is reversed. Experimentally one looks for a shift in the Tl nuclear resonance when the relative direction of the state-selecting magnetic field and the resonance-region electric field is reversed. By time-reversal symmetry, the direction and magnitude of the internal magnetic field is the same for equal and opposite laboratory electric fields in the resonance region.

The measured frequency shift $\Delta\nu$ is given by

$$h\,\Delta\nu = 4d\langle \vec{\sigma}_{\mathrm{Tl}}\cdot\vec{\lambda}_{\mathrm{TlF}}\rangle\ . \tag{2}$$

Figure 1 shows a schematic diagram of the levels involved. Figure 2 shows a schematic diagram of the apparatus. A detailed explanation of the various regions is found in Sec. II. The above-mentioned resonance region is labeled as the C region wherein the Tl nuclear resonance is induced by two separated oscillatory magnetic fields. The state-selecting region is the A region, in which a parallel laboratory magnetic field exists. The B region is analogous to the A region and functions as a Tl spin analyzer, deflecting from the beam only those molecules for which the Tl spin was reoriented in the C-resonance region.

II. OUTLINE OF THE EXPERIMENT

Thallium fluoride was chosen for this experiment for four reasons: (i) The Tl nucleus has spin $\frac{1}{2}$ due to an unpaired proton, (ii) Tl is a high-Z atom, (iii) TlF is a polar diatomic molecule, and (iv) Tl has a low ionization potential. The first criterion allows the experiment to be interpreted in terms of a limit on the proton EDM, the second and third criteria enhance the effective electric field which can be applied to the proton EDM within the Tl nucleus, and the fourth criterion allows for efficient detection of the TlF using a hot-wire detector. The last two criteria suggest a molecular-beam experiment using inhomogeneous electrostatic fields to select the desired rotational state. TlH would actually be a preferable molecule due to the

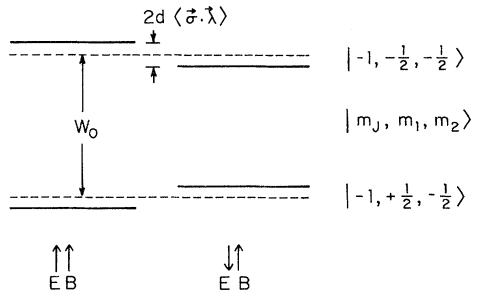

FIG. 1. Schematic diagram of the states involved in the Tl nuclear resonance. The arrows indicate the relative direction of the electric (E) and magnetic (B) fields at the Tl nuclear site, or equivalently, the relative direction of the laboratory fields (i.e., the C-region electric field and the state-selecting magnetic field). The state-selected quantum numbers for molecular rotation (m_J), Tl nuclear spin (m_1), and F nuclear spin (m_2) are shown. The hyperfine energy splitting (W_0) is approximately 120 kHz.

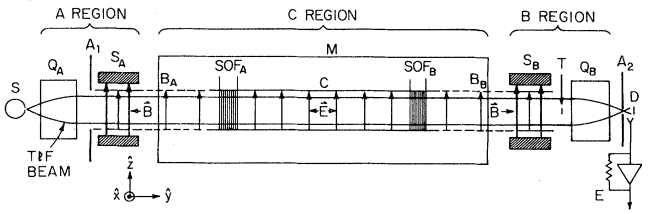

FIG. 2. Schematic diagram of the apparatus with the significant components and regions labeled. S is the thermal effusive source; Q_A, the A-region quadrupole which focuses the $J=1, M_J=0$ rotational states; A_1 is an aperture; S_A, the A subsidiary resonance region wherein the transition $|M_J=0\rangle \rightarrow |-1,-\frac{1}{2},-\frac{1}{2}\rangle$ occurs; B_A, a buffer region to ensure the adiabatic transformation of the states between regions with low and high electric field strengths; SOF_A, the first separated-oscillatory-field coil which induces the Tl nuclear resonance $|-1,-\frac{1}{2},-\frac{1}{2}\rangle \rightarrow |-1,+\frac{1}{2},-\frac{1}{2}\rangle$; C, the high-voltage plates which produce the 20.0 kV/cm electric field in the C region; M, double cylindrical magnetic shields; SOF_B, the second separated-oscillatory-field coil in which the phase of the rf field is $\pm 90°$ with respect to that in SOF_A; B_B, another buffer region; S_B, the B subsidiary resonance region wherein the transition $|-1,-\frac{1}{2},-\frac{1}{2}\rangle \rightarrow |M_J=0\rangle$ occurs; T is a beam stop; Q_B, the B-region quadrupole which focuses the $J=1, M_J=0$ states onto the detector; A_2, a second aperture; D is the hot-wire detector; and E is the electrometer which amplifies the 10^{-10} A beam current.

larger populations one could obtain in the low rotational states; however, it is difficult to make an intense TlH molecular beam.

Figure 2 shows a schematic diagram of the molecular beam along with the physical phenomena taking place in each region. Thallium fluoride is first vaporized in a hot oven forming a thermal beam. The A-region electrostatic quadrupole field is set to state select and focus predominantly the $J=1, m_J=0$ rotational state, leaving the vibrational and electronic states unselected. The $J=1, m_J=\pm 1$ states are deflected out of the beam. High rotational states are selected with poor efficiency. The vibrational-state population in the beam is determined by the thermal-equilibrium distribution at the source temperature. Virtually all beam molecules are in the ground electronic state $^1\Sigma$. The four hyperfine states within the $J=1, m_J=0$ subspace have virtually identical focusing characteristics since they have nearly identical Stark energies (W_s) in the strong electric field of the quadrupoles (the deflecting force is given by $F=-\vec{\nabla}W_s$).

Flipping the Tl spin in the C region corresponds to a hyperfine transition, which does not cause a noticeable change in the beam trajectory when the molecules pass through the B quadrupole. Since the quantum number m_J must change between the A and B quadrupoles in order for molecules originally focused in the A quadrupole ($m_J=0$) to become defocused in the B quadrupole ($m_J=\pm 1$), the above transition is "unobservable." A triple resonance scheme must be used to make the Tl nuclear magnetic resonance observable. This scheme is shown schematically in Fig. 3, where only 3 of the 12 possible hyperfine states are shown for simplicity. The states are

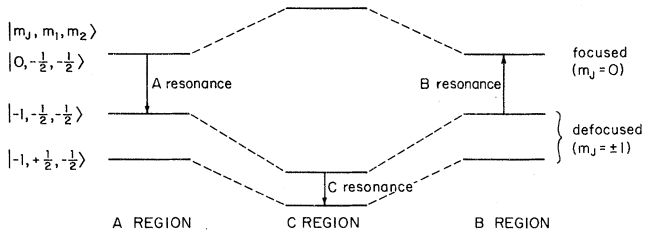

FIG. 3. Triple resonance scheme used to make the Tl nuclear resonance (C resonance) observable. Since the focusing property of the quadrupoles only depends on $|m_J|$, the A and B resonances are used to connect the C resonance with a change in population from an $m_J=0$ state to an $|m_J|=1$ state.

shown with different energies in the C region since this is the case in our experiment. This does not alter the triple resonance scheme provided the molecular states transform adiabatically between the A and B regions, and the C region. If the A and B "subsidiary" resonances in Fig. 3 are tuned to their center frequency, sweeping through the C resonance produces a net transfer of population (on resonance) from the $m_J=0$ hyperfine state to the $m_J=-1$ hyperfine states, thereby leading to an observable change in the focused beam intensity. Furthermore, the A resonance selects a hyperfine state with nonzero m_J which is essential for producing the necessary magnetic field on the Tl nucleus in the C region.

After being rotationally state selected by the A quadrupole, the beam passes into the A subsidiary resonance region (the first in the triple resonance scheme). Here, in the presence of parallel electric (20 V/cm) and magnetic (18.4 G) fields, a transition is made from a $J=1,m_J=0$ hyperfine state to a $J=1,m_J=\pm1$ hyperfine state. Originally this was to be accomplished with a rf electric field oscillating parallel to the static fields (σ transition). However, in the final experiment it was accomplished with nonadiabatic transitions, as explained below. Figure 4 shows the Stark effect for these hyperfine states for low values of the electric field, in the presence of an 18.4 G magnetic field. These eigenvalues were found by diagonalizing the hyperfine Hamiltonian given in Table I for the $J=1$ rotational subspace. The vertical line between level a and level e represents the A and B subsidiary resonances induced by nonadiabatic transitions. Had these transitions been induced by a parallel rf electric field the subsidiary resonances would have connected level a with level j. The Tl nuclear magnetic resonance (C resonance) takes place between level e and level j, although it occurs in the C region at much higher values of the electric field than depicted in Fig. 4 and at zero magnetic field. Table II gives the quantum numbers, in the uncoupled representation, associated with each level.

After passing out of the A subsidiary resonance region the beam enters a buffer region where the electric field strength increases exponentially up to the value found in the C region (20 kV/cm). Magnetic shielding virtually eliminates the earth's magnetic field in the C region (<2 mG). Here the Tl nuclear magnetic resonance is induced. Two separated oscillatory magnetic fields are used for this purpose, oscillating 90° out of phase. The observed reso-

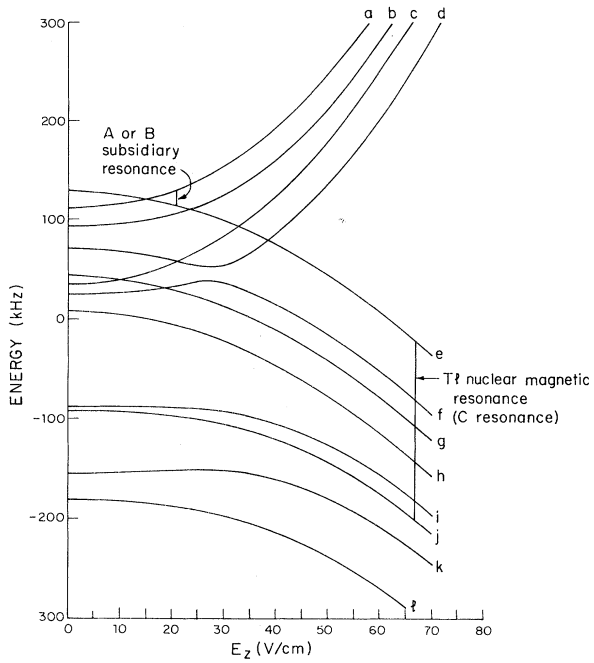

FIG. 4. Stark effect in the $J=1$ rotational subspace of TlF for low values of the electric field and in the presence of a parallel 18.4 G magnetic field. These eigenvalues are appropriate for the fields found in the A and B subsidiary resonance regions ($E_z=20$ V/cm and $B_z=18.4$ G).

nance is shown in Fig. 5.

After the molecules traverse the C region they again pass into a buffer region which ensures the adiabatic transformation of the molecular states between the C region and the B subsidiary resonance region. The B resonance is identical to the A resonance, completing the triple resonance scheme. The beam then passes through the B quadrupole where the $J=1,m_J=0$ hyperfine states are focused onto the hot-wire detector. Here the molecules dissociate and Tl^+ ions are formed to produce a beam signal.

In front of the B quadrupole rests a beam stop which casts a shadow onto the aperture in front of the detector. The purpose of this stop is to block those molecules in the beam which travel straight down the beam axis, undeflected by the quadrupoles. This dramatically reduces the background signal since the molecules of interest ($J=1,m_J=0$) are deflected around the beam stop.

The experiment is performed by tuning to the C-resonance frequency (f_0) and looking for small intensity changes correlated with a reversal of the C-region electric field or with the reversal of the magnetic fields in the two subsidiary resonance regions. These intensity changes are produced by shifts in the resonance frequency. Either one of these operations reverses the relative direction of the electric and magnetic fields at the Tl nucleus in the C region. Reversing the subsidiary magnets selects the opposite magnetic quantum numbers relative to a fixed axis in the C region, thereby reversing the internal magnetic field. It should be noted that when the C-region electric field is

TABLE I. TlF hyperfine Hamiltonian.

$$\mathcal{H}_{\text{hyperfine}}=\mathcal{H}_{\text{rot}}+\mathcal{H}_S+\mathcal{H}_Z+\mathcal{H}_{sr}+\mathcal{H}_{ss}$$

where

$$\mathcal{H}_{\text{rot}}=hB\vec{J}^2$$

$$\mathcal{H}_S=-\vec{\mu}_e\cdot\vec{E}$$

$$\mathcal{H}_Z=-\frac{\mu_J}{J}(\vec{J}\cdot\vec{B})-\frac{\mu_1}{I_1}(\vec{I}_1\cdot\vec{B})-\frac{\mu_2}{I_2}(\vec{I}_2\cdot\vec{B})$$

$$\mathcal{H}_{sr}=c_1(\vec{I}_1\cdot\vec{J})+c_2(\vec{I}_2\cdot\vec{J})$$

$$\mathcal{H}_{ss}=5c_3\left[\frac{3(\vec{I}_1\cdot\vec{J})(\vec{I}_2\cdot\vec{J})+3(\vec{I}_2\cdot\vec{J})(\vec{I}_1\cdot\vec{J})-2(\vec{I}_1\cdot\vec{I}_2)\vec{J}^2}{(2J+3)(2J-1)}\right]+c_4(\vec{I}_1\cdot\vec{I}_2)$$

and

$\vec{J}$ = the rotational angular momentum of the molecule
$\vec{I}_1$ = the Tl nuclear spin
$\vec{I}_2$ = the F nuclear spin
$\vec{E}$ = the external electric field
$\vec{B}$ = the external magnetic field

with[a]

$B=6.689\,92$ GHz	$\mu_e=4.2282(8)$ Debye[b]
$\mu_J=35(15)$ Hz/G	$c_1/h=126.03(12)$ kHz[b]
$\mu_1^{205}=1.2405(3)$ kHz/G	$c_2/h=17.89(15)$ kHz[b]
$\mu_1^{203}=1.2285(3)$ kHz/G	$c_3/h=0.70(3)$ kHz[b]
$\mu_2=2.003\,63(4)$ kHz/G	$c_4/h=-13.30(72)$ kHz.[b]

[a]Reference 12.
[b]These values are for the zeroth vibrational state of ^{205}Tl ^{19}F.

reversed, all other parallel electric fields throughout the apparatus are reversed simultaneously. The quadrupole electric fields are the only ones which do not get reversed.

As noted previously, the A and B subsidiary transitions were not induced by rf electric fields but rather took place automatically due to nonadiabatic transitions occurring between both the A and B quadrupoles and their respective subsidiary resonance regions. These nonadiabatic transitions transferred population, in varying amounts, between the $m_J=0$ hyperfine states (selected by the quadrupoles) and the $m_J=\pm1$ hyperfine states. In retrospect this should not have been so surprising because in these two regions of the apparatus the electric field changes from a high value (1—10 kV/cm) with quadrupole symmetry to the low (20 V/cm) constant field found in the subsidiary resonance regions. Furthermore, the magnetic field changes from the value of the earth's field found in the quadrupole regions to the 18.4 G constant field in the subsidiary resonance-region magnets.

Nonadiabatic transitions, in general, are hard to quantify;[13] however, a qualitative rule of thumb can be given. If two discrete states $|m\rangle$ and $|n\rangle$ of a time-dependent Hamiltonian are coupled, then, in order for the nonadiabatic transitions between the two states to be negligible, the time during which the interaction between the states changes appreciably must be long compared to $2\pi/\omega_{mn}$ (the inverse of the Bohr frequency between these two

TABLE II. Table of the eigenvectors that are the major components of the designated states at the fields used in the experiment.

Level	$\lvert m_J,m_1,m_2\rangle$
a	$\lvert 0,-\frac{1}{2},-\frac{1}{2}\rangle$
b	$\lvert 0,+\frac{1}{2},-\frac{1}{2}\rangle$
c	$\lvert 0,-\frac{1}{2},+\frac{1}{2}\rangle$
d	$\lvert 0,+\frac{1}{2},+\frac{1}{2}\rangle$
e	$\lvert -1,-\frac{1}{2},-\frac{1}{2}\rangle$
f	$\lvert +1,+\frac{1}{2},-\frac{1}{2}\rangle$
g	$\lvert -1,-\frac{1}{2},+\frac{1}{2}\rangle$
h	$\lvert +1,+\frac{1}{2},+\frac{1}{2}\rangle$
i	$\lvert +1,-\frac{1}{2},-\frac{1}{2}\rangle$
j	$\lvert -1,+\frac{1}{2},-\frac{1}{2}\rangle$
k	$\lvert +1,-\frac{1}{2},+\frac{1}{2}\rangle$
l	$\lvert -1,+\frac{1}{2},+\frac{1}{2}\rangle$

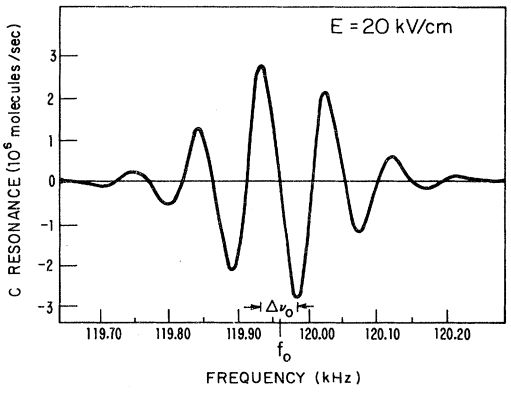

FIG. 5. Observed Tl nuclear resonance (C resonance) induced by separated oscillatory fields 90° out of phase.

states). In the regions of the apparatus between the quadrupoles and the subsidiary resonance regions, parallel and perpendicular time-varying electric and magnetic fields exist. These time-dependent fields couple all the hyperfine states in one way or another. Given an average beam velocity of 1.3×10^4 cm/s, the frequency of these time-varying fields is ~10 kHz, which is high enough to cause numerous nonadiabatic transitions.

Efforts to eliminate these transitions were not successful so we decided to turn them to our advantage by using them to induce the A and B subsidiary resonances instead of using rf electric fields. This worked quite well because of the fortuitous circumstance that one state (level j in Fig. 4) was relatively unpopulated by nonadiabatic transitions, for reasons which were never fully understood, whereas the companion state for the C resonance (level e) was populated copiously. This happy circumstance provided a relatively strong C resonance, from which we estimate a transition probability of approximately 0.5 for both the A and B subsidiary resonance. The other three candidates for a C resonance were of much smaller intensity and could not be augmented by the application of rf electric fields in the subsidiary regions, indicating that both levels for these transitions were saturated. Therefore, the Tl nuclear magnetic resonance used in the experiment was $|-1,-\frac{1}{2},-\frac{1}{2}\rangle\rightarrow|-1,+\frac{1}{2},-\frac{1}{2}\rangle$.

Though it at first seems strange to use nonadiabatic transitions in the triple resonance scheme, there is nothing wrong with it in principle, provided they perform the essential functions of the A and B resonances. Since the C-resonance frequency is determined solely by the magnitude of the laboratory electric field in the C region, the state-selection process cannot affect this frequency. We further verified that the proper directions for the electric and magnetic fields at the Tl nuclear site were obtained in the C region when the laboratory electric and magnetic fields were reversed. However, nonadiabatic transitions affect the state populations, which in practice turned out to be a nuisance. When the laboratory fields were reversed, the C-resonance amplitude changed by as much as 20%. By adjusting the electric field in the subsidiary regions (20 ± 5 V/cm) and, more importantly, by adding Helmholtz coils to cancel the magnetic field of the earth in the regions between the quadrupoles and the subsidiary resonance regions, these amplitudes changes were reduced to 1% and were often as low as 0.2% (magnetic shielding would have been better, but this was impossible given the present construction of the apparatus).

III. APPARATUS

Table III summarizes some of the important parameters in the experiment.

A. Vacuum system

The main vacuum system was pumped by oil-diffusion pumps using DC 705 pump oil. Only the detector region used ion pumps. The vacuum achieved throughout the apparatus was $\sim4\times10^{-8}$ torr, although the detector region was brought up to 1×10^{-6} torr by bleeding O_2 into the system to oxidize partially the detector surface, and thereby to increase its ionization efficiency.

TABLE III. Typical values for experiment parameters.

Source intensity (at 380°C)	2×10^{16} molecules/sr sec
Total beam intensity (I_{tot})	3×10^8 molecules/sec
C-resonance intensity (I_{res})	4×10^6 molecules/sec
Average beam velocity	1.3×10^4 cm/sec
C-resonance frequency (f_0 at 20.0 kV/cm)	119.952 kHz
C-resonance FWHM ($\Delta\nu_0$)	45 Hz
TlF oven temperature	380°C
Quadrupole voltage	±4.0 to ±5.0 kV
Subsidiary region electric field	20 V/cm
Subsidiary region magnetic field	18.4 G
C-region electric field	20.0 kV/cm
C-region magnetic field	<2 mG
Hot-wire detector efficiency	0.85
Source-to-detector distance	450 cm
Separation between separated-oscillatory-field coils	144 cm
Beam diameter	1.5 cm

B. Source

The source was a modified effusive design. TlF salt is contained in the lower half of a double chambered 6 in.×5/8 in. oxygen-free, high-conductivity (OFHC) copper tube, indirectly heated to 380°C by passing 30 A of ac current through a concentric thin-walled stainless steel tube surrounding the Cu tube. The lower chamber is separated from the upper chamber by a plate with a 0.020 in. hole in it. The upper chamber is empty and has a 0.100 in. hole in the side for the TlF vapor to escape, thus forming the beam. Placed in the lower chamber along with the TlF salt is a corrugated OFHC Cu sheet which acts as a "boiling chip," smoothing out thermal instabilities in the hot salt melt. This helped steady the beam intensity.

The double chambered source served two functions. Originally it was designed to further stabilize the beam intensity, with the upper chamber acting a bit like the capacitor in an RC filter. However, it also helps reduce the fraction of TlF dimers in the beam. Dimers are objectionable because they do not contribute to the C resonance, yet they contribute two Tl^+ ions to the background signal. A normal (single chambered) effusive TlF source produces a beam consisting of 75% dimers and 25% monomers. With the double-chambered source we were able to shift this to 38% dimers and 62% monomers. This occurs because, for the same temperature, the vapor in the upper chamber is at a lower pressure than in the lower chamber. The exact value depends on the ratio of the hole diameter in the plate separating the two chambers to the diameter of the exit hole (1:5 in the present design). According to Le Chatlier's principle the dissociation reaction

$$(TlF)_2\rightleftarrows2TlF$$

shifts to the right in the upper chamber, enhancing the monomer fraction in the vapor and consequently in the beam.

At a temperature of 380°C this source produced C-resonance intensities of 4×10^6 molecules/sec (see Table III). At higher temperatures the source produced beams up to 20 times as intense. These high intensity beams were never used in the experiment because they caused excessive high-voltage breakdown due to rapid salt buildup on the high-voltage insulators in the C region (a problem which could have been fixed had the extra intensity been needed).

It should be noted that since the vapor in the source is in thermal equilibrium, many rotational and vibrational states will be populated. At 380°C approximately 8×10^{-5} of the TlF molecules are in a given hyperfine state in the zeroth vibrational, $J=1$ subspace.

C. Quadrupoles

The rotational state selection of the beam is accomplished by electrostatic quadrupoles. The deflecting force $\vec{F}$ arises from the interaction between the gradient of the electrostatic field and the induced electric dipole moment of the molecule and is given by

$$\vec{F}=-\vec{\nabla}W_s=-\frac{dW_s}{dE}\vec{\nabla}E\ ,$$

where W_s is the Stark energy for a given rotational state (see Fig. 6) and E is the magnitude of the electric field. If the electric field is sufficiently small, the Stark energy will be a quadratic function of E, in which case the molecules execute simple harmonic motion in the plane perpendicular to the quadrupole axis as they traverse its length. In order for focusing to occur, one designs the quadrupoles in such a way that molecules emanating from a source aligned along the axis at the entrance of the quadrupole exit from the far end after executing one-quarter cycle of their radial motion, i.e., the radial velocity is brought to a halt. Despite the simplicity of this result for the quadratic Stark effect, higher intensity focused beams can be obtained using stronger electric fields. For molecules in the $J=1, m_J=0$ state, six times the focused beam is obtained using shorter quadrupoles with electric fields up to $\lambda=5$ ($\lambda\equiv\mu E/hB$) compared to longer quadrupoles with $\lambda<1$ which produce for simple harmonic motion.[14]

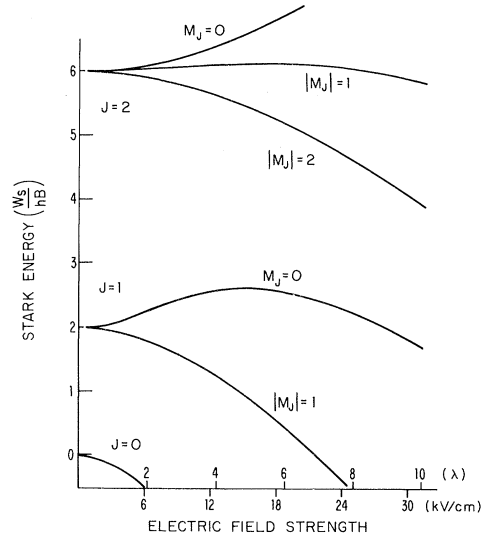

FIG. 6. Stark energy of a rigid rotator as a function of the electric field strength. The values given in kV/cm apply to TlF, whereas λ is the dimensionless field strength ($\lambda\equiv\mu E/hB$, where μ is the molecular electric dipole moment, E is the electric field strength, h is Planck's constant, and B is the rotational constant of the molecule). The hyperfine splitting for TlF is too small to show on this scale.

Another important feature of the quadrupole design is that it selects molecules whose average velocity is 0.5 times the most probable beam velocity given by the Maxwell velocity distribution. This counterintuitive design actually increases the focused beam intensity because at slower beam velocities the solid angle of the source which can be focused initially increases more rapidly than the probability for finding molecules with this beam velocity decreases. Furthermore, selecting slower molecules narrows the C-resonance linewidth.

Physically the quadrupoles are constructed from 3/4 in. stainless steel rods, 11.5 in. in length, centered on the corners of a square 0.988 in. on a side. Typical voltages on the rods were between ±4.0 and ±5.0 kV, with adjacent rods being oppositely charged.

D. Subsidiary resonance regions

These regions consists of parallel electric and magnetic fields. An electromagnet, made with a soft iron yoke, is magnetized with 0.75 A of dc current passed through 104 windings. This produces an 18.4 G field across a 2.1 cm gap, homogeneous to within 1% over the central 5 cm of its 8 cm length. By reversing the current, the field reverses to within 1%. The electric field was produced by placing ±15 V across two parallel plates separated by 1.5 cm. A parallel rf electric field could be superimposed upon this constant field to induce the subsidiary transitions resonantly, however, as described above, this rf field was not used since these transitions were induced nonadiabatically.

E. C region

Before entering and after exiting the C region, the beam passes through buffer regions which consist of a series of six parallel plates, oppositely charged with exponentially increasing voltage steps. This allows the molecular states to transform adiabatically from the low electric field values found in the subsidiary regions to the high electric field in the C region.

In the C region two long (208 cm×6.5 cm) parallel anodized Al plates are oppositely charged to ±15.00 kV. The 1.50 cm separation provided a 20.0 kV/cm electric field homogeneous to within 1% and reproducible to within 0.01%. The anodized aluminum was intended to prevent breakdown between the plates. It accomplished this. However, due to the insulating anodized layer, surface charges built up on the plates giving rise to stray electric fields on the order of 2 V/cm, which did not reverse completely upon reversal of the high voltage. To first order this could be canceled by adding a battery in series with

the high voltage on one of the plates.

The two separated-oscillatory-field coils used to drive the C resonance were made from 81 turns of teflon-coated wire wrapped along a 9 in. glass tube of rectangular cross section. The coils slipped over the ends of the high-voltage plates without touching. A 25 mA rms rf current produced the axial oscillatory magnetic field necessary to optimize the Tl nuclear magnetic resonance (0.6 transition probability). The long length of the separated-oscillatory-field coils minimized any frequency shift arising from the Millman effect.[15]

F. Detector

The beam was detected by a standard hot-wire detector consisting of a tungsten ribbon heated to 930 °C in a partial vacuum of 1×10^{-6} torr O_2 (which was bled into the detector region through a nozzle pointed at the active area of the tungsten ribbon). The oxygen forms a surface layer of tungsten oxide which has a higher work function than pure tungsten metal. With its high work function, the oxide surface has a greater affinity for the outer Tl electron than the atom (I.P.$=6.106$ eV). Consequently, when the TlF molecule dissociates on the hot wire and the Tl atom evaporates from the surface, it does so as an ion.[16] The ionization efficiency for TlF on our hot wire was measured to be 0.85 ± 0.02. The ions are collected on a nearby metal plate biased 8 V negative with respect to the hot wire, ensuring nearly 100% collection efficiency. An electrometer then amplifes the 10^{-10} A ion current to form the beam signal.

The tungsten ribbon for the hot wire was made by heating a tantalum ribbon in a partial vacuum (200 μ) of tungsten hexacarbonyl $W(CO)_6$.[17] This causes pure tungsten metal to be deposited on the tantalum substrate through the decomposition of $W(CO)_6$ on the hot surface. Making tungsten ribbons in this fashion was necessitated by the fact that virtually all commercially available tungsten (even high purity, "undoped" tungsten) contains trace amounts of potassium. When such tungsten is used to make hot wires, large K^+ background signals are observed. The homemade tungsten ribbons had backgrounds $<10^{-12}$ A, i.e., $<1\%$ of the beam signal.

G. Magnetic shielding

Two concentric cylinders (one made from Mumetal and the other from Hipernom) were used to shield the C region, by a factor of 2600, from external magnetic fields. Small magnetic hard spots in the stainless steel vacuum chamber (located inside the magnetic shields) were only partially degaussed with a 1000 G rms ac magnetic induction. These residual fields together with the leakage of the magnetic field of the earth through the ends of the cylindrical magnetic shields resulted in a field on the order of 2 mG averaged over the C region. As a result, Helmholtz coils were used to trim out any nonzero z component of the magnetic field (the component parallel to the C-region electric field) so that when the subsidiary magnets were reversed, the C resonance did not change frequency.

H. Data collection

The experiment was controlled by a Digital Equipment Corporation PDP-8/E computer which selected the various states of the experiment, monitored error conditions, and collected the raw data from which we determined C-resonance frequency shifts. The computer, in conjunction with several homemade interfaces, operated as a multichannel lock-in detector.[18]

The computer controlled four parameters: (1) the phase of the current in the second separated-oscillatory-field coil relative to the first ($\pm90°$), (2) the direction of the magnetic field in the subsidiary resonance regions, (3) the direction of the electric field along the beam line, i.e., the C-region electric field, and (4) the frequency applied to the C-resonance coils. Setting these parameters defines a given state of the experiment. After waiting an appropriate amount of time for transients to die out, a gate opens for a fixed length of time (typically 50.0 ms) to count an input frequency derived from the electrometer signal through a voltage-to-frequency converter. The accumulated number of counts represents the integrated beam signal for that state of the experiment. If no error indications occurred in taking this data, the computer sets the next state of the experiment, waits for transients to die out, then integrates the beam signal in this new configuration.

The manner in which three of the four parameters are controlled is illustrated in Fig. 7, where S_P, S_M, and S_E represent the pattern for phase reversal, magnet reversal, and electric field reversal, respectively. By adding the integrated beam signal when the phase-reversal waveform S_P is $+1$ ($+90°$) and subtracting when the waveform is -1 ($-90°$), a total is accumulated which represents the magnitude of the C resonance at the frequency set by the computer since only the number of resonated molecules is affected by a change in the phase of the separated oscillatory fields. If the electric (or magnetic) field is reversed in

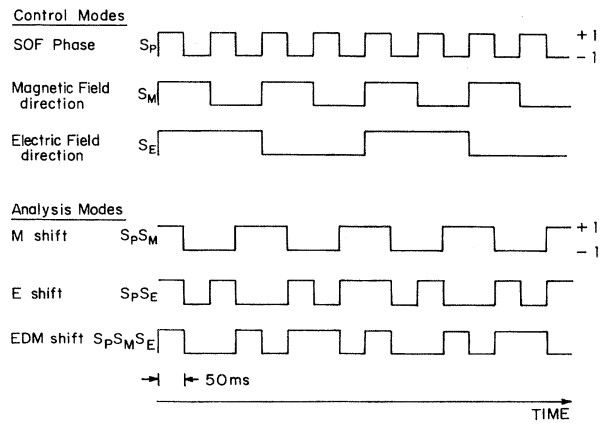

FIG. 7. Examples of possible control and analysis modes for the experiment. The control modes show the pattern in which a given variable could be modulated. The analysis modes show patterns which extract various correlated beam-intensity changes from the data. The actual experiment was run with more complicated modes than those shown here to improve noise immunity. SOF stands for separated oscillatory field.

a different pattern, S_E (or S_M), and the data is added or subtracted according to whether the product waveform $S_P S_E$ (or $S_P S_M$) is $+1$ or -1, then the accumulated number is proportional to the shift in the C resonance under a reversal of the electric (or magnetic) field. Such frequency shifts are called "E shifts" (or "M shifts") and they served as important diagnostics throughout the experiment. Finally, if one adds or subtracts the incoming data according to the product waveform $S_P S_M S_E$ one obtains a number proportional to the shift in the C resonance when only the relative direction of the laboratory electric and magnetic fields is reversed. This is the analysis mode which checks for a P- and T-violating frequency shift, and as such is called the "EDM shift." To calibrate the C-resonance slope a small shift in the separated-oscillatory-field frequency is introduced by the computer and the corresponding change in the number of resonated molecules is observed. The measured slope is then used to transform the counts accumulated as E shifts, M shifts, and EDM shifts into equivalent frequency shifts.

The actual experiment was run with more complicated modes than those represented in Fig. 7. For instance, the separated-oscillatory-field phase was actually reversed with the pattern labeled $S_P S_M S_E$ in Fig. 7. These more complicated waveforms provided increased immunity from systematic effects due to drifts in the beam signal. The general noise-rejection properties of these waveforms are discussed by Harrison *et al.*[18] The separated-oscillatory-field phase was the most rapidly modulated parameter, with the highest frequency component of the waveform being $\simeq 7$ Hz. The magnetic field direction was the next most rapidly modulated parameter (~ 1 Hz) and the electric field changed no faster than once every 15 seconds.

The error conditions monitored throughout the experiment were of three kinds. First, voltages and currents were monitored to make sure that not only were the electric and magnetic fields in the direction specified by the computer, but that the magnitudes of these fields were within 1% of their nominal value (the high voltage for the C-region electric field was specified to be within 2% of its nominal value). Second, all vacuum ionization gauges were monitored to make sure that there were no abnormal pressure fluctuations in the vacuum system. Third, the electrometer was monitored for any rapid spikes on the output voltage, indicating abnormal beam fluctuations. If none of the above error conditions occurred while the beam signal was being integrated, the data was accepted by the computer. These checks are to some extent redundant. For instance, a spark from the high-voltage plates in the C region causes the high voltage to fluctuate outside the 2% window and causes the vacuum pressure to increase rapidly, thus causing a sudden attenuation of the molecular beam due to pressure scattering. Consequently, all three error flags go up when a spark occurs. One further check is performed by the computer once the data has been accepted. The incoming integrated beam signal is compared to the last value to see that it has not changed by more than 3%. If it has, the data is rejected. This checks for slower changes in the beam intensity which are often missed by the discriminator which looks for the rapid spikes. Having passed all the error checks, the "good" data is then binned up according to the various analysis modes corresponding to E shifts, M shifts, EDM shifts, and several other modes which serve to check for spurious results in the data.

IV. EXPERIMENT SENSITIVITY

The precision with which small frequency shifts $\delta\nu$ can be observed is determined by requiring that the intensity change,

$$\delta I = \frac{dI}{d\nu}\delta\nu \,, \tag{3}$$

be larger than the noise. Operating at the zero crossing of the C resonance (f_0) maximizes $dI/d\nu$. For the separated-oscillatory-field line shape $dI/d\nu \simeq I_{\rm res}/\Delta\nu_0$, where $I_{\rm res}$ is the resonant amplitude and $2\Delta\nu_0$ is the separation between adjacent interference fringes. If the experiment runs for a time $T/2$ with the electric and magnetic fields parallel, and then for $T/2$ with the fields antiparallel, the accumulated count proportional to an EDM shift is $T/2\ \delta I$. The fluctuation in this number is given by Poisson statistics as $(TI_{\rm tot})^{1/2}$ where $I_{\rm tot}$ is the total beam arriving at the detector (resonance plus background). The condition for an observable frequency shift is then given by

$$\delta\nu \geq \frac{2\Delta\nu_0}{I_{\rm res}}\left[\frac{I_{\rm tot}}{T}\right]^{1/2} . \tag{4}$$

In this experiment a 10 h run should have produced a resolution $\delta\nu \geq 2$ mHz (see Table III). In fact the resolution was more like 4 mHz due to other sources of noise.

V. RESULTS

This section summarizes different frequency shifts in the Tl nuclear resonance when the laboratory fields were reversed. A "shift" was defined as a change in the number of resonated molecules under a reversal of a given laboratory field. Using the measured C-resonance slope, this was converted to an equivalent frequency shift in Hz (for small frequency shifts). However, it is worth noting that if the separated-oscillatory-field frequency is not set to the zero crossing of the Tl nuclear resonance (f_0), then changes in the resonance amplitude under field reversal will also give rise to changes in the number of resonated molecules, consequently contributing to a "frequency shift." In this manner shifts in the C-resonance frequency were monitored when the subsidiary magnets were reversed (M shift) and when the C-region electric field was reversed (E shift). A shift which depended solely on the relative direction of these laboratory electric and magnetic fields was labeled the EDM shift. Since spurious EDM shifts were observed in the experiment, Sec. V D is devoted to a summary of various mechanisms by which a false EDM shift can occur.

A. M shifts

Originally an M shift on the order of 10 Hz was observed which was attributed to a residual 2 mG magnetic

field. This shift was canceled to the level of 100 mHz by the addition of Helmholtz coils the length of the C region. Another source for an M shift is the Millman effect.[15] The Millman effect is the shift in a resonance frequency due to the spatial curvature of the oscillatory field inducing the transition. Only one of the two rotating fields, into which an oscillatory field can be decomposed, is responsible for inducing the transition. In the rest frame of the beam molecule, this rotating component will either be increased or decreased in frequency depending on which way the oscillatory field bends. When the magnetic field is reversed the opposite rotating component is responsible for inducing the transition. The result is an apparent change in the resonant frequency under magnetic field reversal. While this description pertains to a single oscillatory field, a very similar phenomenon occurs for separated oscillatory fields. Here the average angle of rotation of the oscillatory fields between the two regions is the relevant spatial rotation which, combined with the time of flight between the two coils, determines the frequency shift of the separated-oscillatory-field line shape. In this experiment the upper limit for any separated-oscillatory-field Millman effect was 1.5 Hz. Since the effect of a real magnetic field cannot be distinguished from the Millman effect, as long as the beam velocity is not reversed, their relative contribution to the observed M shift was indeterminate at the level of 1-Hz shifts. For the purposes of this experiment the M shift was empirically nulled to better than 100 mHz (and was often as low as 10 mHz) by tuning the C-region Helmholtz coil. Fluctuations in the M shift between 10 and 100 mHz can be attributed to 2–20 μG changes in the magnetic field (z component).

B. E shifts

E shifts are analogous to M shifts except that they are correlated with the reversal of the electric field in the C region. Typical E shifts were on the order of 200 mHz. They arose predominantly from stray charges on insulating surfaces which did not change sign when the voltage was reversed. The observed E shift implies a 2 V/cm nonreversing electric field since the electric field dependence of the C resonance is 41 Hz/kV/cm. A variable 10 V potential placed in series with the high voltage to one of the plates canceled the E shift to first order. However, due to the erratic nature of these stray electric fields, the E shift also fluctuated between 10 and 100 mHz.

C. EDM shift

A convenient way to define EDM shifts experimentally is as the difference between the M shift with one direction of the electric field and the M shift with the opposite direction of the electric field. The difference between E shifts with opposite magnetic fields is equivalent.

Figure 8 shows the EDM shifts for the Tl nuclear resonance in two different TlF rotational states. The error bars represent the standard deviation of the mean for the observed EDM shifts in a given run. In general this reflects random noise on the beam signal (about twice the theoretical shot noise); however, sometimes the EDM shift was found to drift over time, in which case the error bar also reflects this drift. The different size standard deviations essentially reflect differences in the total number of molecules collected. The results taken in the $J=2$, $m_J=-2$ state correspond to the transition $|m_J=-2,m_1=-\frac{1}{2},m_2=-\frac{1}{2}\rangle \rightarrow |-2,+\frac{1}{2},-\frac{1}{2}\rangle$, with a resonant frequency $f_0=246.46$ kHz. While this resonance has not been previously mentioned, one observes it in exactly the same way as the $J=1,m_J=-1$ resonance, however, the quadrupole voltage is increased to focus the $J=2$ rotational states more effectively. One should note that the reference to J is intended only as a label identifying the low field origin of the state, since J is not a good quantum number in high electric fields. The last runs using the $J=1,m_J=-1$ resonance represent the cleanest data since most of the systematic effects had been eliminated and the resonance amplitude changes under electric and magnetic field reversals were held to a minimum ($\lesssim 1\%$).

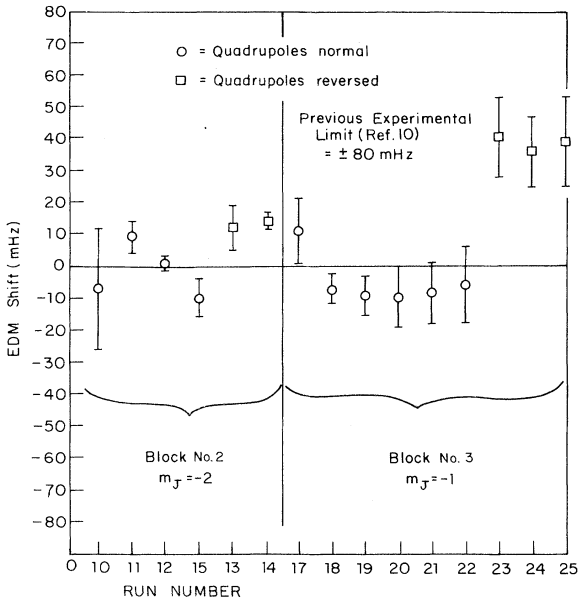

FIG. 8. Experimental values for the EDM shift. Note that the data represents two different rotational states of TlF and two different polarities of the A and B quadrupole voltage.

The $m_J=-1$ results clearly show the remaining systematic change in the EDM shift when the quadrupole voltage was reversed. In principle such a reversal should not have any effect on the experiment since the state selecting and focusing properties of the quadrupoles is determined solely by the gradient of the magnitude of the electric field. However, the direction of the fringe electric fields will reverse which can affect the nonadiabatic transitions occurring between the quadrupoles and their respective subsidiary resonance regions, consequently affecting the hyperfine state selection efficiency. Even so, it is hard to see how this can affect the C resonance in such a way as to lead to an EDM shift. Table IV gives the weighted mean of the EDM shift for the two rotational states, separated according to quadrupole field direction.

TABLE IV. Summary of EDM shift results.

Transition	Quadrupole direction	Weighted mean
$M_J=-1$	normal	-6.3 ± 3.1mHz
	reversed	38 ±7 mHz
$M_J=-2$	normal	1.1 ± 1.6 mHz
	reversed	13.8 ± 2.4 mHz

D. Systematic EDM effects

Unfortunately no explanation was found for the remaining systematic EDM shifts. Numerous mechanisms were proposed, several of which were important in reducing systematic EDM shifts early in the experiment, but none seemed capable of explaining the large 44-mHz change in the EDM shift observed in the $M_J=-1$ data, or the 13-mHz change observed in the $M_J=-2$ data.

From the definition of the EDM shift given above one should realize that any mechanism which produces an E shift or an M shift can produce a spurious EDM shift if the magnitude of that shift changes when the other field reverses direction. In other words, if some mechanism produces a 100 mHz M shift with the electric field in the $-\vec{E}$ direction and only 80 mHz when the electric field is in the $+\vec{E}$ direction, then a spurious EDM shift of 20 mHz will result.

Perhaps the best known systematic EDM shift for experiments of this kind is the frequency shift induced by the magnetic moment of the particle (neutron or Tl nucleus) interacting with the motional magnetic field $\vec{E}\times\vec{v}/c$ observed in the rest frame of the particle as it passes through the high electric field region. The interaction Hamiltonian

$$\mathcal{H}=-2\mu_1\vec{I}_1\cdot(\vec{E}\times\vec{v}/c) \tag{5}$$

changes sign under a reversal of the relative direction of the electric and magnetic fields ($\vec{I}_1$ reverses with $\vec{B}$), consequently masquerading as a true EDM shift. To cancel this effect one should reverse the beam velocity; however, in practice this is difficult. Alternatively one can eliminate this effect by making the electric and magnetic fields parallel at the Tl nucleus. In this experiment this is guaranteed by quantum mechanics, as was described previously. However, an external magnetic field will destroy this perfect alignment, which is the main reason for the magnetic shielding around the C region. A stray magnetic field as large as 50 mG, perpendicular to the internal magnetic field, produces a systematic EDM shift of 0.2 mHz which is entirely negligible in the present experiment.

A second mechanism for producing a systematic EDM shift arises when the C resonance changes in amplitude under magnetic (electric) field reversal and the resonance shifts in frequency under electric (magnetic) field reversal. To see this one only needs to realize that if the amplitude of the resonance, and hence the resonance slope, changes under magnetic (electric) field reversal, the number of counts which accumulate as an E shift (M shift) differs depending on the direction of $\vec{B}$ ($\vec{E}$). Therefore a nonzero EDM shift appears. It was for this reason that changes in the resonant amplitude were minimized under electric and

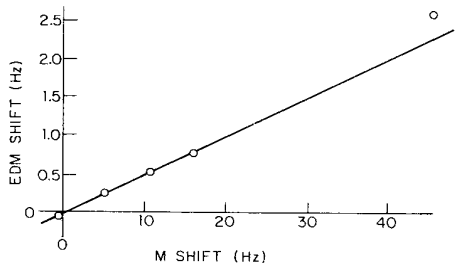

FIG. 9. Spurious EDM shift induced by a large M shift.

magnetic field reversals. The signature for this systematic effect is, (1) it is proportional to the magnitude of the E or M frequency shift, (2) it is proportional to the percentage change in the resonant amplitude, and (3) it is proportional to the resonance amplitude itself, which implies that the effect is frequency dependent. The proportionality between this induced EDM shift and the M shift is shown in Fig. 9, for an amplitude change $\simeq10\%$ under electric field reversal. Figure 10 shows the linear frequency dependence over a frequency range where the resonance line shape is linear. Finally, in Fig. 10 one should notice the reduction by a factor of 10 in the slope of this EDM shift when the resonance amplitude change is reduced by a factor of 10. Reducing the amplitude change to $\lesssim1\%$, reducing the E and M shifts to below 100 mHz, and operating at the zero crossing of the line shape, together constrain any systematic EDM shift arising from this mechanism to be $\lesssim2$ mHz.

Another possible source for a systematic EDM shift comes from overlapping transitions. If, in fact, the observed zero crossing of the ^{205}Tl nuclear resonance was ac-

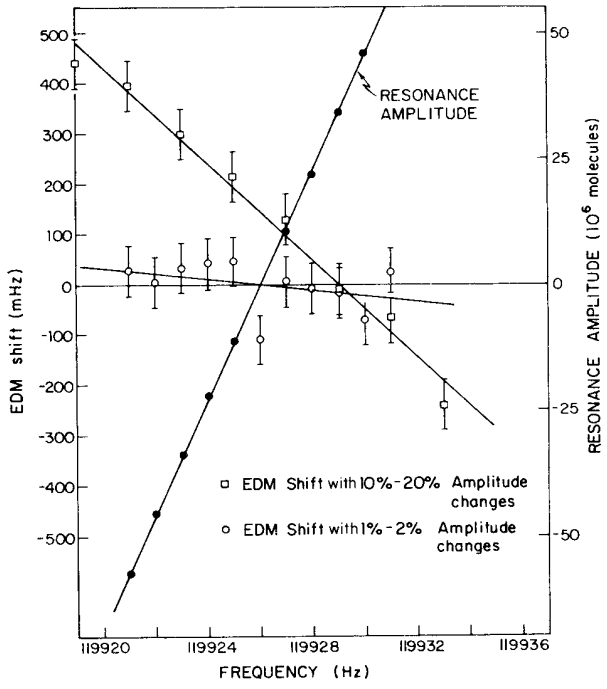

FIG. 10. Frequency and amplitude change dependence of a spurious EDM shift. The lines represent least-squares fits to the data.

tually the cancellation of small overlapping transitions and this main resonance, then any difference in the amplitude changes for the overlapping transitions appear as frequency shifts in the main resonance. In particular, if the amplitude changed when the relative field direction is reversed, as was often observed for the main resonance, then this "EDM amplitude change" appears directly as an EDM shift in the main resonance. Candidates for overlapping transitions are as follows.

(1) The "time-reversed" transition, $|+1,+\frac{1}{2},+\frac{1}{2}\rangle \rightarrow |+1,-\frac{1}{2},+\frac{1}{2}\rangle$, whose states are degenerate with those of the main C resonance ($|-1,-\frac{1}{2},-\frac{1}{2}\rangle \rightarrow |-1,+\frac{1}{2},-\frac{1}{2}\rangle$) in a pure electric field. In principle the state $|+1,+\frac{1}{2},+\frac{1}{2}\rangle$ should not be selected in the triple resonance scheme, however, since the subsidiary transitions are induced nonadiabatically this state is inadvertantly populated. In fact, the time-reversed transition occurred at exactly the same frequency but with 10% of the amplitude of the main resonance. By applying a small magnetic field (100—200 mG) the length of the C region, which reversed when the subsidiary magnets reversed, this overlapping transition was separated out. There was no resulting change in the systematic EDM shift, acquitting this suspect.

(2) The C resonance between the states $|-1,-\frac{1}{2},-\frac{1}{2}\rangle$ and $|-1,+\frac{1}{2},-\frac{1}{2}\rangle$ which belong to the $J=2$ rotational subspace occurs at almost exactly the same frequency as the corresponding $J=1$ transition. By lowering the quadrupole voltage, fewer $J=2$ molecules are selected relative to the more easily focused $J=1$ molecules. Consequently, any effect of the overlapping $J=2$ transition should be a strong function of the magnitude of the quadrupole voltage. No effect was observed.

(3) The ^{203}Tl, $J=1, m_J=-1$ C resonance in the zeroth vibrational state and the ^{205}Tl, $J=1, m_J=-1$ transition in the first vibrational state both lie ~ 1 kHz below the main resonance. The wings of these transitions could conceivably influence the zero crossing of the main resonance, however, it is unlikely given the amplitude of these transitions 1 kHz away from their center frequency (the separated oscillatory field envelope has a half-width $\simeq 150$ Hz). Furthermore, the oscillations in the separated-oscillatory-field line shape change with the average beam velocity, which can be altered to some extent by changing the quadrupole voltage. Consequently, changing the quadrupole voltage would vary the amount to which these overlapping transitions contributed to the observed zero crossing of the main resonance. As mentioned above, changing the magnitude of the quadrupole voltage had no effect.

(4) Finally, we checked for a nonresonant background signal that possibly changed amplitude in an EDM fashion. Sampling the background at frequencies where no resonance occurs produced no significant EDM shift at the level of 10 mHz.

Nonlinearities in the C resonance near the zero crossing can also produce systematic EDM shifts if both E shifts and M shifts occur during the run. In this case, the number of counts corresponding to the E shift change when the magnetic field reverses because the M shift places you on a different part of the resonance slope. The zero crossing of the C resonance is linear to better than 1% which, when combined with worst case E and M shifts equaling 100 mHz, produces a negligible systematic EDM shift (0.1 mHz).

A rather different mechanism for producing a false EDM shift arises from a change in the average transverse beam position under magnetic (or electric) field reversal (due to a change in the cross-sectional beam-intensity profile) in conjunction with a transverse gradient in any nonreversing component of the electric (or magnetic) field in the C region. Changes in the cross-sectional beam profile do not seem unlikely when one recalls that the hyperfine state selection occurs via nonadiabatic transitions, the efficiency of which can vary across the beam profile depending on the details of the time-varying fields along each trajectory between the quadrupoles and their respective subsidiary resonance regions. A nonreversing electric field in the C region (due to static charges, for instance) gives rise to an E shift. Therefore a gradient to this nonreversing field implies that this E shift changes when the average beam position moves under magnetic field reversal. Consequently, a false EDM shift will result. Checking for such effects produced a limit of 1 mHz on any systematic EDM shifts so generated.

This is unfortunate because this last mechanism would have explained the influence of the reversal of the quadrupole voltage since reversing the quadrupole voltage changes the fringe electric fields between the quadrupoles and the subsidiary resonance regions, thus potentially affecting the cross-sectional profile of the nonadiabatic transitions, and consequently the average beam position. With the beam in this new position the spurious EDM shift generated by the above mechanism would quite likely be different.

Finally, in an effort to identify other potential mechanisms for generating systematic EDM shifts, a number of parameters were varied and their effect on the EDM shift observed. No significant effect was found. The parameters were (1) the dead time which allows transients to die out after the state of the experiment has been switched, (2) the "frequency" of the modulation waveforms which control the experiment; (3) the phase accuracy of the second separated-oscillatory-field coil with respect to the first (normally it is $\pm 1°$), and (4) the reduction of miscellaneous sources of electric noise.

In summary, no mechansim was found which could explain the observed systematic EDM shifts, much less the large change in these shifts when the quadrupole voltage was reversed. Table V summarizes the mechanisms discussed above.

VI. CONCLUSIONS

Since the systematic change in the EDM shift under quadrupole reversal is by far the dominant source of error, and since to date we have no reliable explanation for its origin, we have little choice but to quote error bars which accommodate this systematic effect. A simple averaging

TABLE V. Table of systematic EDM shifts.

Mechanism	EDM shift
$\vec{E}\times\frac{\vec{v}}{c}$	<0.2 mHz
Resonant amplitude changes	$\lesssim 2$ mHz
Amplitude changes in overlapping transitions	<10 mHz
Off-resonant EDM background	<10 mHz
Nonlinearities of the resonant line shape	$\lesssim 0.1$ mHz
Spatial shifts in the average beam	
Under $\vec{B}$ reversal	$\lesssim 1$ mHz
Under $\vec{E}$ reversal	<1 mHz
Transient effects	negligible
Separated-oscillatory-field phase error	$\lesssim 0.5$ mHz

of the results for opposite quadrupole voltages yields a nonzero EDM shift which cannot be trusted. Thus, reasonable values for the two sets of data are

$$\delta\nu_{\rm EDM}=16\pm25 \text{ mHz} \quad (m_J=-1)$$

and

$$\delta\nu_{\rm EDM}=7\pm10 \text{ mHz} \quad (m_J=-2)$$

where $\delta\nu_{\rm EDM}$ is the EDM shift. The two results are handled separately because molecules in the $J=2, m_J=-2$ state have a different polarizability in the C-region electric field. Using Eq. (2) we find the following values for d:

$$\frac{d}{h}=9\pm14 \text{ mHz} \quad (m_J=-1)$$

and

$$\frac{d}{h}=6\pm9 \text{ mHz} \quad (m_J=-2)$$

where we have used the values $\langle\vec{\sigma}\cdot\vec{\lambda}\rangle=0.46$ and 0.27 for the polarization of TlF in a 20.0 kV/cm electric field for the $J=1$ and $J=2$ rotational states, respectively.

Since the errors inherent in these results are systematic rather than statistical, it makes little sense to take the weighted mean for the final result. Instead we simply average the results along with the errors. This *ad hoc* procedure attempts to reflect the greater reliability of the $m_J=-1$ data along with the lower systematic errors observed in the $m_J=-2$ data. The final result is taken to be

$$\frac{d}{h}=8\pm12 \text{ mHz}. \tag{6}$$

From the calculations of Hinds and Sandars,[10] d can be related to the value of a proton EDM, D_p. Including both the finite size effect and the magnetic effect discussed earlier for measuring the EDM of charged particles, they find that

$$\frac{d}{h}=5.9\times10^{18}D_P \text{ Hz}, \tag{7}$$

where D_P is measured in e cm. Combining Eq. (6) with Eq. (7), we find the following limit for the proton EDM:

$$D_P=(1.3\pm2.0)\times10^{-21}\ e \text{ cm}. \tag{8}$$

Equation (8) is to be compared to the present experimental limit quoted by Hinds and Sandars,[10] $D_P=(1.8\pm7)\times10^{21}$ e cm.

Since calculating the finite size effect relies on uncertain nuclear integrals, a more cautious estimate of an upper limit would only include the magnetic effect, in which case

$$\frac{d}{h}=8.5\times10^{17}D_P \text{ Hz}.$$

This puts the inferred proton EDM value at

$$D_P=(9\pm14)\times10^{-21}\ e \text{ cm}.$$

Alternatively an EDM shift can be attributed to a P- and T-violating neutral-current tensor interaction between protons and electrons, of the form

$$\mathcal{H}_T=iC_T\left[\frac{G_F}{2^{1/2}}\right]\bar{\psi}_p\Gamma_T\psi_p\bar{\psi}_e\Gamma_T\psi_e\delta(\vec{r}_e-\vec{r}_p),$$

where Γ_T is the antisymmetric combination of Dirac matrices. Again, Hinds and Sandars have shown that if the entire effect is attributed to a neutral-current tensor interaction,

$$\frac{d}{h}=(1.4\times10^3)C_T \text{ Hz}. \tag{9}$$

When combined with the result of this experiment [Eq. (6)] we find a new null result for C_T,

$$C_T=(6\pm9)\times10^{-6}. \tag{10}$$

The previous result was $C_T=(0.8\pm3)\times10^{-5}$.[10]

The statistical resolution for observing frequency shifts in the Tl nuclear resonance was better than 1 mHz in this experiment. By modifying the apparatus to eliminate the systematic EDM shift, and by using the high beam intensities that were obtained (but never used), along with longer running times ($\gtrsim 100$ h), one could hope to observe EDM shifts on the order of 0.1 mHz. This would imply a limit on the proton EDM of $\sim1\times10^{-23}$ e cm. Consequently, there remains a factor of 100 to be gained from the present experimental approach to P and T violations in the hyperfine structure of TlF.

[1]J. H. Christenson, J. W. Cronin, V. L. Fitch, and R. Turlay, Phys. Rev. Lett. 13, 138 (1964).
[2]E. M. Purcell and N. F. Ramsey, Phys. Rev. 78, 807 (1950).
[3]W. B. Dress, P. D. Miller, J. M. Pendlebury, P. Perrin, and N. F. Ramsey, Phys. Rev. D 15, 9 (1977).
[4]I. S. Altarev *et al.*, Phys. Lett. 102B, 13 (1981).
[5]L. I. Schiff, Phys. Rev. 132, 2194 (1963).
[6]P. G. H. Sandars, in *Atomic Physics IV*, edited by G. Putlitz,

E. W. Weber, and W. Winaacker (Plenum, New York, 1975).
[7]P. G. H. Sandars, Phys. Lett. 14, 194 (1965); 22, 290 (1966); Phys. Rev. Lett. 19, 1396 (1967); J. Phys. B 1,(2), 499 (1968); 1,(2), 511 (1968).
[8]M. A. Player and P. G. H. Sandars, J. Phys. B 3, 1620 (1970).
[9]G. E. Harrison, P. G. H. Sandars, and S. J. Wright, Phys. Rev. Lett. 22, 1263 (1969).
[10]E. A. Hinds and P. G. H. Sandars, Phys. Rev. A 21, 471 (1980); 21, 480 (1980).
[11]E. A. Hinds, C. E. Loving, and P. G. H. Sandars, Phys. Lett. 62B, 97 (1976).
[12]H. Dijkerman, W. Flegel, G. Gräff, and B. Mönter, Z. Naturforsch. Teil A 27, 100 (1972).
[13]A. Messiah, *Quantum Mechanics,* Vol. II (Wiley, New York, 1958); L. I. Schiff, *Quantum Mechanics* (McGraw-Hill, New York, 1968).
[14]D. Wilkening, Ph.D. thesis, Harvard University, 1981 (unpublished).
[15]N. F. Ramsey, *Molecular Beams* (Oxford University, New York, 1956).
[16]S. Datz and E. H. Taylor, J. Chem. Phys. 25, 389 (1956); H. Lew, in *Methods of Experimental Physics, 4A,* edited by V. W. Hughes and H. L. Schultz (Academic, New York, 1967); É. Ya. Zandberg and N. I. Ionov, Usp. Fiz. Nauk 67, 581 (1959) [Sov. Phys.—Usp. 2, 255 (1959)].
[17]J. W. Frazer, R. P. Burns, and G. W. Barton, Rev. Sci. Instrum. 30, 370 (1959); E. F. Greene, *ibid.* 32, 860 (1961).
[18]G. E. Harrison, M. A. Player, and P. G. H. Sandars, J. Phys. E 4, 750 (1971).